

# The Tricontinuous $3ths(5)$ Phase: A New Morphology in Copolymer Melts

Michael G. Fischer,<sup>†,‡,§</sup> Liliana de Campo,<sup>‡,||</sup> Jacob J. K. Kirkensgaard,<sup>⊥</sup> Stephen T. Hyde,<sup>‡</sup> and Gerd E. Schröder-Turk<sup>\*,†,‡</sup>

<sup>†</sup>Institut für Theoretische Physik, Friedrich-Alexander Universität Erlangen-Nürnberg, Staudtstr. 7B, 91058 Erlangen, Germany

<sup>‡</sup>Applied Maths, Research School of Physics & Engineering, The Australian National University, Canberra ACT 0200, Australia

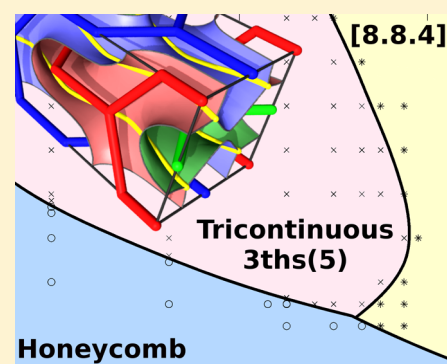
<sup>§</sup>Adolphe Merkle Institute, Chemin des Verdiers 4, CH-1700 Fribourg, Switzerland

<sup>||</sup>Australian National Science and Technology Organisation, Bragg Institute, New Illawarra Road, Lucas Heights NSW 2234, Australia

<sup>⊥</sup>Niels Bohr Institute, University of Copenhagen, Universitetsparken 5, 2100 København, Denmark

## Supporting Information

**ABSTRACT:** Self-assembly remains the most efficient route to the formation of ordered nanostructures, including the double gyroid network phase in diblock copolymers based on two intergrown network domains. Here we use self-consistent field theory to show that a tricontinuous structure with monoclinic symmetry, called  $3ths(5)$ , based on the intergrowth of three distorted  $ths$  nets, is an equilibrium phase of triblock star-copolymer melts when an extended molecular core is introduced. The introduction of the core enhances the role of chain stretching by enforcing larger structural length scales, thus destabilizing the hexagonal columnar phase in favor of morphologies with less packing frustration. This study further demonstrates that the introduction of molecular cores is a general concept for tuning the relative importance of entropic and enthalpic free energy contributions, hence providing a tool to stabilize an extended repertoire of self-assembled nanostructured materials.



The cubic gyroid structure<sup>1,2</sup> of symmetry  $Ia\bar{3}d$ , with two intergrown highly symmetric network domains, is a ubiquitous complex network phase in soft matter, with a plethora of applications as a functional nanomaterial.<sup>3</sup> It forms spontaneously in biological and synthetic systems,<sup>2</sup> including block copolymers,<sup>4–7</sup> and is a useful template for metallic and inorganic replicas.<sup>8</sup> The double gyroid and its chiral single-network counterpart of symmetry  $I4_132$  (formed e.g. in membrane-templated nanostructures in insects<sup>9</sup>) have demonstrated photonic,<sup>10,11</sup> plasmonic,<sup>12,13</sup> mechanical and transport,<sup>14</sup> electrochromic,<sup>15</sup> or photovoltaic<sup>16</sup> functions, all of which are essentially determined by their network-like morphology. In amphiphilic systems, the gyroid and related network phases form as the result of a delicate balance between interface tension and packing considerations.<sup>17</sup> The interfaces are related to negatively curved triply periodic minimal surfaces, resulting in bicontinuous morphologies with two compartments with network-like topology.

The existence of bicontinuous morphologies suggests the possibility of network-like *tricontinuous* structures, based on three intergrown network-like domains. We here consider *balanced* tricontinuous morphologies, where the three domains are of identical shape and their backbones given by the same three-periodic net. The dividing surface between three intergrown nets necessarily contains *triple lines* (shown in yellow in Figures 1 and 3), along which all three network

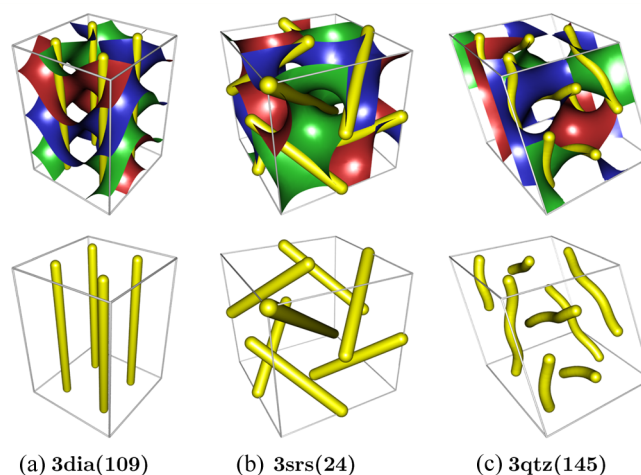


**Figure 1.** Candidate morphologies for tricontinuous mesophases with three intergrown network domains. Yellow lines are triple lines, which define the loci of the molecular centers and along which all three domains meet.

**Received:** August 8, 2014

**Revised:** October 3, 2014

**Published:** October 23, 2014

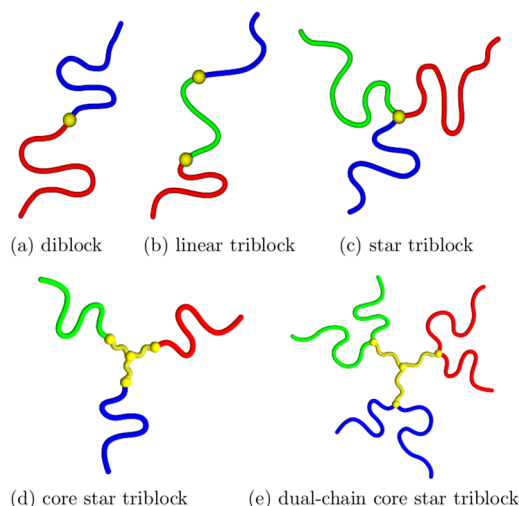


**Figure 2.** Different linear and star-copolymer architectures, with and without an extended core.

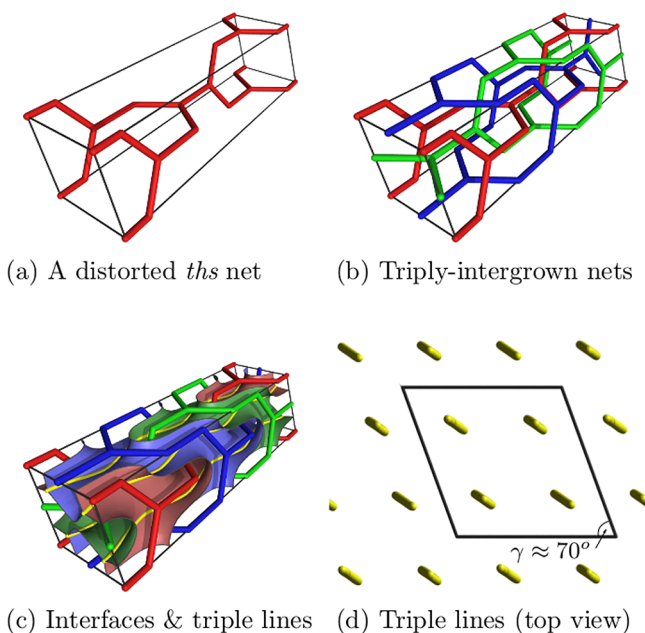


**Figure 3.** Geometry of the  $3ths(S)$  phase. (a) Each component  $A$ ,  $B$ , and  $C$  is represented by a distorted monoclinic version of the  $ths$  net. (b) Three  $ths$  nets can be intergrown to give the  $3ths(S)$  structure of symmetry group  $I112$ , with  $c/a \approx 4.5\text{--}9.5$ . (c) Interfaces between the copolymeric components can be illustrated by minimal surface patches that meet along the triple lines which represent the location of the core  $X$ . (d) The triple lines revolve around straight lines along the crystallographic  $c$ -axis that are arranged approximately on a triangular lattice.

domains meet; the interface is otherwise composed of curved surface patches (modeled as minimal surfaces) between pairs of the three graphs. Numerous tricontinuous structure models have been described.<sup>18–25</sup>

Tricontinuous morphologies in amphiphilic systems had been proposed theoretically.<sup>24,26</sup> They became a likely experimental reality with the discovery of the solid IBN-9 mesoporous silicate<sup>27</sup> and have very recently been found experimentally in gemini surfactants.<sup>28</sup> However, the partition of space into a triplet of locally adjacent networks suggests self-assembly via a different molecular architecture, namely from

star-shaped molecules with three immiscible arms,<sup>29</sup> each arm forming a network-like domain and the molecular cores lying on triple lines. Three-arm molecules have been shown (by simulation<sup>29–32</sup> and experiment<sup>33</sup>) to form a simple hexagonal columnar phase based on the [6.6.6] tiling, referred to here as *hexagonal honeycomb* (unless the molecular structure enforces a spontaneous twist between adjacent molecules<sup>18</sup>); cf. Figures 4d and 5a. So far, stable balanced tricontinuous phases have not been found in studies of three-arm polyphile molecules in solution<sup>34</sup> or in triblock star-copolymers,<sup>33</sup> or in blends thereof.<sup>35</sup>

We show here that the introduction of an extended core into the molecular architecture of triblock star-copolymers breaks the free energetic advantage of the columnar hexagonal honeycomb phase, resulting in the tricontinuous phase, termed  $3ths(S)$ , based on three intergrown 3D nets, labeled  $ths$  in ref 36 (Figure 3).

### ■ THERMODYNAMIC STABILITY AT INTERMEDIATE SEGREGATION STRENGTHS

Spectral self-consistent field theory (SCFT) calculations<sup>37</sup> (see also Supporting Information section II) are used to obtain free energy estimates and equilibrium mesophase morphologies,<sup>38</sup> for incompressible melts of star-copolymers assuming that the polymeric components are Gaussian chains. The SCFT equations for the density profiles  $\rho_K(\vec{r})$  of the copolymeric components  $K$  are solved in Fourier space by the Anderson mixing scheme<sup>39</sup> for a given morphology, providing in particular the free energy  $F$  and the equilibrium length scale  $\xi$  (for which  $F$  is minimal). Each morphology is encoded as a set of crystallographic basis functions (see Supporting Information section II.C). The equilibrium phase is identified as the morphology which gives the lowest free energy value.

We consider the molecular architectures for star-copolymers<sup>40</sup> composed of three polymeric species illustrated in Figure 2. A *balanced triblock ABC star-copolymer*, henceforth referred to as *star-copolymer*, consists of three polymeric chains  $A$ ,  $B$ , and  $C$ , with equal monomer numbers  $N_A = N_B = N_C = N/3$  and with pairwise identical repulsive interaction strength  $\chi = \chi_{AB} = \chi_{AC} = \chi_{BC}$  per monomer; the chains are covalently linked together at a common junction, the molecular center (Figure 2c). A (single-chain) *core star-copolymer* (Figure 2d) is obtained by replacing the junction with a star-copolymer, called the *extended core*, with three identical arms of component  $X$ . The volume fraction of the core is  $f_X = N_X/(N + N_X)$  where  $N_X$  is the monomer number of the core. The repulsive interaction strength per monomer between  $X$  and the copolymeric chains is  $\chi_X = \chi_{AX} = \chi_{BX} = \chi_{CX}$ . A *dual-chain core star-copolymer* (Figure 2e) consists of the same core  $X$ , where each arm is connected to a pair of  $A$ ,  $B$ , or  $C$  chains, each of length  $N/6$ .

Our key result is the phase diagram (Figure 4) for dual-chain core star-copolymers which includes significant parameter regions for which the tricontinuous  $3ths(S)$  structure is the stable equilibrium phase. This phase forms at core volume fractions  $f_X$  around 20% when the segregation strength  $\chi_X$  between the core  $X$  and the three chains  $A$ ,  $B$ , and  $C$  is sufficiently strong. The phase is adjacent to the conventional honeycomb columnar phase<sup>33</sup> at lower core volume fraction  $f_X$  or lower segregation ratios  $\chi_X/\chi$  and to another new columnar phase for larger core volumes. Including the polygons representing the core domains, the conventional honeycomb corresponds to the [12.12.3] tiling. For weak segregation of the

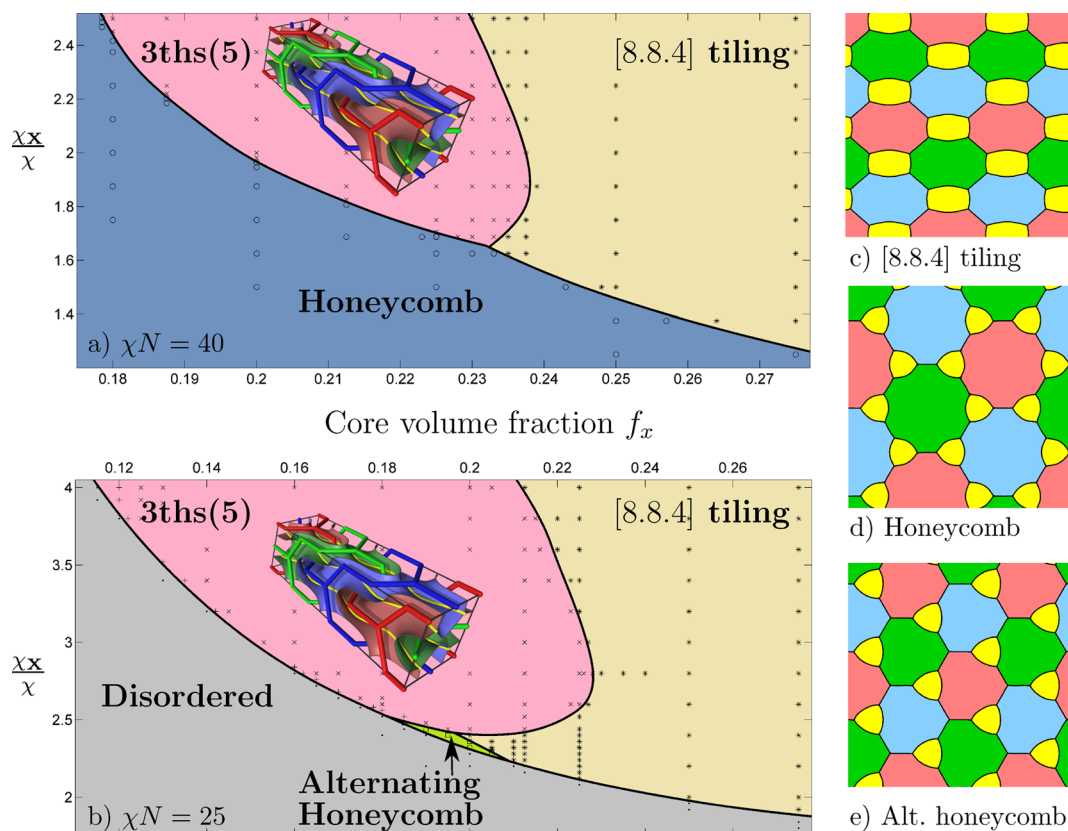


**Figure 4.** Phase diagram of dual-chain core star-copolymers for different segregation strengths  $\chi N = 40$  (a) and  $\chi N = 25$  (b): Data points are results from SCFT simulations, each representing the minimal free-energy phase. See Supporting Information sections II and V for details on the calculation of the phase diagram. (c–e) Representations of the SCFT observed profiles for the three observed columnar phases; at each point, the color represents the component  $K$  with the maximal density value  $\rho_K(\mathbf{r})$  out of the four components  $K = A, B, C,$  and  $X$ . Note the deviations of the core regions from a spherical cross section. (c)  $\chi N = 40, f_X = 0.25, \chi_X/\chi = 2$ ; (d)  $\chi N = 40, f_X = 0.2, \chi_X/\chi = 1.625$ ; (e)  $\chi N = 25, f_X = 0.2, \chi_X/\chi = 2.36$ . See Supporting Information section V for complete representation of phase data. The “disordered” phase is a spatially homogeneous fluid state of all four components (see Supporting Information section II.H).

ABC chains ( $\chi N \approx 25$ , Figure 4b), this novel tricontinuous phase is adjacent to the order–disorder transition.

The *3ths(5)* phase is *tricontinuous* (following the definition of ref 18); each of the copolymeric domains  $A, B,$  and  $C$  forms a single connected (mathematically speaking “continuous”) network-like labyrinthine domains, all of identical shape. Each domain is described by a periodic net that is a monoclinic distortion of the *ths* net.<sup>36</sup> In common with the nets in the gyroid and  $O70$  phases,<sup>41,42</sup> three edges emanate from each vertex and the smallest cycles are 10-rings. The *3ths(5)* structure has monoclinic symmetry  $I112$  (space group number 5 in ref 43) with only a single 2-fold axis. The ratio of the crystallographic lattice parameters is large, around  $c/a \approx 4.5$ – $9.5$ , and the angle between the  $a$ - and  $b$ -axes is  $\gamma \approx 70^\circ$ – $75^\circ$ , depending on  $\chi N$  as well as on  $f_X$  and  $\chi_X$ .<sup>a</sup> The fourth component, the core  $X$ , forms an infinite array of discrete helical rods parallel to the crystallographic  $c$ -axis, each representing a triple line.

The phase diagram further contains another new columnar phase, based on the *distorted [8.8.4] Archimedean tiling* and of symmetry  $cm$  (wallpaper group no. 5) (see Figures 4c and 5d). In this phase, the cross sections of the  $A, B,$  and  $C$  domains are distorted octagons (that in the limit of small cores become  $60^\circ$  rhombi), four of which are arranged around each triple line: two of one material and one of each of the others. In the equilibrium copolymer morphology, the quadrilateral cross

sections of the core domains are elongated (Figure 4).<sup>b</sup> (Undistorted [8.8.4] tilings, where the cores are not arranged on a triangular lattice, have been observed in star-copolymeric melts.<sup>33,44</sup>) For weaker segregation strengths  $\chi N = 25$ , an additional columnar phase, termed the *alternating honeycomb*, is found to be stable in a narrow parameter range. However, near the order–disorder transition thermal fluctuations (neglected by the mean-field SCFT theory) are important, making the existence of the alternating honeycomb phase less certain.

The identification of the equilibrium phases rests on comparison of free energies of different test morphologies, computed by spectral SCFT. Our set of test morphologies include the columnar and tricontinuous morphologies detailed in Table 1, lamellar, micellar, and striped lamellar morphologies (see Supporting Information sections II.D, IV, and V).

Note that the *3ths(5)*, the distorted [8.8.4] tiling, and the alternating honeycomb phase share the common feature that the triple lines trace lines (straight or slightly curved) approximately arranged on a triangular lattice.

The key ingredient to the stabilization is the enhanced entropic chain stretching effect due to introduction of the extended core  $X$ . As the limit of small core volumes in the phase diagrams shows (see Figure 4 and Supporting Information section II.G), the *3ths(5)* phase is not stable anywhere in the phase diagram of single- or double-chain star-copolymers without a core. The use of double-chain rather than

**Table 1. Structural Data and Free Energy Terms for the Candidate Mesophase Morphologies for Star-Copolymer Self-Assembly<sup>a</sup>**

structure	symmetry	<i>c/a</i>	$\gamma$	$A_{ABC}/(LV)^{1/2}$	$L/V\langle z^2 \rangle$
honeycomb	$p3m1$			1.32	0.192
3cds(1)	$P1$			1.61	0.179
3ths(109)	$I4_1md$	4.5		1.62	0.174
3ths(5)	$I112$	4.5	70	1.63	0.167
3srs(24)	$I2_12_12_1$			1.78	0.166
3qtz(145)	$p3_2$	1.3		1.89	0.162
alternating honeycomb	$p^3$			1.86	0.160
6-fold tiling	$p^2$			2.15	0.160
distorted [8.8.4] tiling	$cm$			2.15	0.160

<sup>a</sup>Each structure is labeled following the notation of ref 36, with the space group number in parentheses. Where necessary, structural parameters (*c/a* ratio, angles of the unit cell) are chosen as the values corresponding to optimal choices in the numerical SCFT calculations. Note that the data for  $\langle z^2 \rangle$  is obtained neglecting the particular curved shape of the interfaces (see Supporting Information section III.A.2). Note the general tendency that an increase in the interface term  $A_{ABC}/(LV)^{1/2}$  is accompanied by a lower stretching term  $L\langle z^2 \rangle/V$ . The family 3ths(109) contains 3dia(109) as a special case.

single-chain core star-copolymers is a further necessary contribution to the stability of this phase. In single-chain core star-copolymers, the 3ths(5) phase is not stable for any value of  $f_X$  (see Supporting Information section II.G).

An alternative to the use of double-chain core star-copolymers that would also likely stabilize the 3ths(5) phase is the use of single-chain core star-copolymers with different statistical segment lengths for the chains that constitute the core and those that constitute the ABC chains. The strong segregation theory suggests this because changing the molecular architecture or the statistical segment lengths alter the stretching free energies (cf. eq 3) in a similar way.

### ■ THE ROLE OF THE EXTENDED CORE IN EMPHASIZING CHAIN STRETCHING, ELUCIDATED IN THE STRONG SEGREGATION LIMIT

The identification of the 3ths(5) structure as a stable tricontinuous phase in star-copolymer melts confirms the intuition gained from the following geometric analysis in the strong segregation limit. In short, the introduction of an extended core into the molecular architecture increases the relative contribution of chain stretching entropy (or packing frustration) relative to interfacial surface tension. This mechanism is sufficient to break the prevalence of the hexagonal columnar honeycomb phase and to tip the balance between interface and chain stretching terms to favor the 3ths(5) phase which has less chain stretching frustration but higher surface area than the conventional honeycomb.

The strong segregation theory<sup>45</sup> (SST) is the limiting case of SCFT, where one considers infinite immiscibility and hence sharp interfaces between the chemically different components. While SCFT presents the overarching numerical framework applicable to all segregation strengths, the SST allows for the derivation of analytic equations that express the thermodynamic free energy as a function of explicit geometric properties (surface areas, volumes, width homogeneity) of the copolymeric interfaces and domains. In the SST limit, the free energy per copolymer

$$\frac{F}{nk_B T} = \frac{F_{\text{Int}}}{nk_B T} + \frac{F_{\text{Conf}}}{nk_B T} \quad (1)$$

consists of a surface tension term,  $F_{\text{Int}}/nk_B T = O(1/\xi)$ , where  $\xi$  is length scale of the structure. The chain stretching term,  $F_{\text{Conf}}/nk_B T = O(\xi^2)$ , penalizes configurations that require a high degree of chain stretching in order for the polymeric chains to fill space and fulfill the incompressibility constraint. The surface tension term favors minimal interfacial areas and decreases as  $1/\xi$  as the structural length scale  $\xi$  increases, hence favoring larger structural lengths, whereas the chain stretching term grows as  $\xi^2$  with  $\xi$ , hence favoring smaller length scales. The length scale of the equilibrium structure is the result of minimizing eq 1 with respect to  $\xi$ .

For the cases of single- and double-chain star-copolymers without a core, the surface tension term reads<sup>46</sup>

$$\frac{F_{\text{Int}}}{nk_B T} = Na\sqrt{\frac{\chi}{6}} \frac{A_{ABC}}{V} = O(1/\xi) \quad (2)$$

where  $A_{ABC}$  is the combined surface area of all interfaces between distinct species within one unit cell;  $V$  is the unit cell volume, and  $a$  is the statistical segment length of each component.

The stretching term reads<sup>47</sup>

$$\frac{F_{\text{Conf}}}{nk_B T} = \sum_{K \in \{A, B, C\}} \frac{3\pi^2}{8f_K^2 Na^2 V} \int_{V_K} d^3r z^2(\vec{r}) = O(\xi^2) \quad (3)$$

where  $f_K$  is 1/3 for star-copolymers with three single chains (Figure 2c) and 1/6 for the case with pairs of chains.<sup>48</sup> The integral in (eq 3) is performed over the regions  $V_K$  occupied by the respective species  $K$ .  $z(\vec{r})$  can be thought of as the distance from a point  $\vec{r}$  along the shortest coarse-grained polymer path (in the configuration that minimizes  $F_{\text{Conf}}$  while obeying the incompressibility constraint) from the volume element at  $\vec{r}$  to its associated grafting point. While this complex definition of  $z$  prevents the exact evaluation of  $F_{\text{Conf}}$  except for in the simpler mesophase morphologies,<sup>49</sup> approximate expressions discussed below provide estimates for the degree of chain stretching frustration.

The equilibrium morphology is determined by the minimization of  $F$  in eq 1 with respect to different candidate morphologies and to the structural length scale  $\xi$  (see Supporting Information section III). As stated above, the resulting equilibrium length scale is a compromise between the tendency of the surface tension term to increase  $\xi$  and the stretching term to decrease  $\xi$ .

Importantly, it turns out<sup>38</sup> that this minimization always leads to a length scale  $\xi$  such that the ratio  $F_{\text{Conf}}/F_{\text{Int}}$  is

$$\frac{F_{\text{Conf}}}{F_{\text{Int}}} = \frac{1}{2} \quad (4)$$

providing the relative weight of the two terms in the equilibrium length scale (see Supporting Information section III.D).

For star-copolymers without extended molecular cores, the structure minimizing this free energy is the hexagonal columnar phase, a honeycomb structure with triple lines at all hexagon corners (Figure 5a).

However, while optimal with respect to interface area, the honeycomb structure has a significant degree of chain stretching frustration. This is best illustrated by the cross-

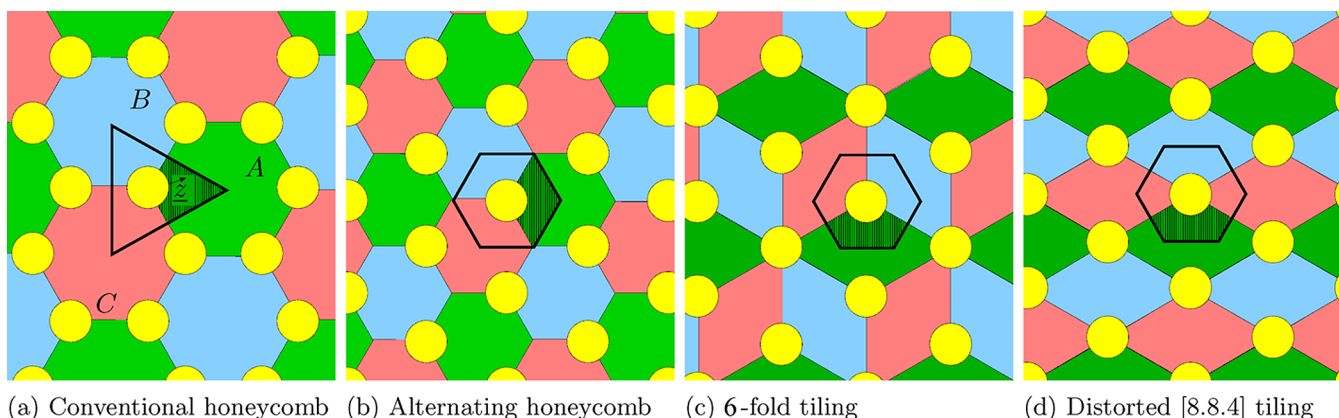


**Figure 5.** Candidate morphologies for columnar phases. Black polygons delineate the spatial regions associated with a given triple line (yellow) and hatched regions the volume domain  $V_A$ . The combined cross section of the domains  $V_A$ ,  $V_B$ , and  $V_C$  of the conventional honeycomb is a triangle, in contrast to the hexagonal domain cross sections of the alternating honeycomb (b), of the 6-fold tiling (c) and of the distorted [8.8.4] tiling (d). Compared to the triangular shape of the conventional honeycomb, their hexagonal shapes are significantly closer to a segment of a cylinder around the triple line, yielding lower values of  $L\langle z^2 \rangle/V$  and hence lower chain stretching. This effect becomes more pronounced for larger cores. Note that the triple line arrangements in (b–d) contain the same triangular lattice.

sectional area available to the A, B, and C chains of a star-copolymer whose core sits at a triple line: its triangular shape is far from the ideal isotropic (circular) shape with constant radius. Evidently, circular disks do not tile space without gaps and therefore cannot be realized in copolymeric melts. The most nearly circular shape that can form a periodic space-tiling system is the hexagon that results if the triple lines are arranged on a triangular lattice, e.g., in the columnar phases in Figure 5b–d and in approximate form also in the tricontinuous *3ths(5)* morphology.

This qualitative argument corresponds to the quantitative inference that when assuming a fixed triple line length  $L$  per unit cell and a fixed unit cell volume  $V$  (which together fixes the length scale  $\xi$ ), the packing term  $L\langle z^2 \rangle/V$  is minimal when the domain  $V_K$  occupied by copolymer component  $K = A, B$ , and  $C$  is a segment of a cylinder with radial isotropy (see Supporting Information sections III.B, III.C, and IV). Any deviation from the cylindrical shape increases  $L\langle z^2 \rangle/V$ , i.e., the packing frustration. The alternating honeycomb, the 6-fold tiling, and the distorted [8.8.4] tiling (Figure 5b–d) have lower stretching frustration  $L\langle z^2 \rangle/V$  than the conventional honeycomb structure (Table 1). Similarly, the packing frustration of those tricontinuous morphologies whose triple lines follow triangular or other close-packed lattices adopts intermediate values (Table 1). These considerations clearly emphasize the importance of the arrangement of the triple lines on a close-packed lattice to minimize packing frustration.

However, for star-copolymers without an extended core, the small interface term of the conventional honeycomb at the equilibrium length scale outweighs its larger chain stretching frustration.

In order to stabilize the tricontinuous phase (with less stretching frustration but larger interfaces), it is necessary to pronounce the role of the stretching term relative to the surface tension term. This effect is achieved by any mechanism that prevents the system from reducing its structural size: At larger length scales, the contribution of the stretching term to the free energy is larger relative to the surface tension term, thus favoring structures with lower degrees of chain stretching.

While the length scale could be constrained explicitly by specific molecular interactions (see Supporting Information

section III.C.1), we achieve a similar effect by the introduction of an extended core  $X$ . Its primary effect is the creation of additional interfaces (between A and X, B and X, and C and X) that increase the surface area. The stretching contribution of the core star-copolymer is still largely described by eq 3 (see Supporting Information section III.C.2). The surface tension term (eq 2) now reads

$$\frac{F_{\text{int}}}{nk_B T} = Na \left[ \sqrt{\frac{\chi}{6}} \frac{A_{ABC}}{V} + \sqrt{\frac{\chi_X}{6}} \frac{A_X}{V} \right] \quad (5)$$

where  $A_X$  denotes the combined interface area between the core  $X$  and  $K = A, B$ , and  $C$ .<sup>c</sup>  $F_{\text{int}}$  increases when the volume fraction  $f_X$  of the core  $X$  or the segregation strength  $\chi_X$  increase. The resulting equilibrium length scale  $\xi$  (at which  $F_{\text{int}} = 2F_{\text{Conf}}$ ) can become larger when compared to the case without the core. This results in a relatively stronger chain stretching contribution, which in turn stabilizes the tricontinuous *3ths(5)* phase and the [8.8.4] tiling.

While these geometric arguments were developed for the strong segregation regime, the predicted phase sequence of conventional honeycomb, tricontinuous *3ths(5)* phase, and [8.8.4] tiling is also observed in the SCFT calculations for intermediate segregation strengths (Figure 4), adding further support to the general validity of this geometric picture.

## DISCUSSION AND CONCLUSION

The theoretical analysis of this article now calls for experimental attempts to realize the tricontinuous *3ths(5)* phase. Since the purpose of the core is simply the creation of additional interfaces near the triple lines, a variety of realizations are conceivable, e.g., via the introduction of aromatic cores<sup>50</sup> or nanoparticle–polymer composites.<sup>51</sup> The unit cell size can be shielded from shrinkage by e.g.  $\pi$  stacking<sup>50,52</sup> or H-bonding of cores,<sup>50,53</sup> thereby also emphasizing the stretching contributions. Maximal stiffness of the core (that suppresses the entropic contributions of the core) and strong interactions  $\chi_X$  between the core and the other components aid stability.

The *3ths(5)* phase challenges the notion that systems driven toward structural homogeneity—here by virtue of the packing term—tend to adopt highly symmetric morphologies; in soft

bicontinuous phases this notion has been reinforced through the ubiquity of the cubic bicontinuous phases, where the high symmetry is however a consequence of homogeneity.<sup>54</sup> The 3ths(S) phase, and the  $O^{70}$ <sup>41,42</sup> phase of symmetry *Fddd*, demonstrate that packing homogeneity can be achieved without high three-dimensional crystallographic symmetry. On the practical side, the low monoclinic symmetry of the 3ths(S) phase with large ratios of the lattice parameters emphasizes the caution that simulation studies in cubic or rectangular simulation boxes fail to observe low-symmetry morphologies.

Our results reinforce the role of geometry for the study of nanomaterials. Geometric intuition has here provided a shortcut to the design of a fundamentally new nanostructure, bypassing the details of chemical composition or physical interactions and the pitfalls of molecular simulations. Geometric analyses, recognized for the understanding of the bicontinuous structures,<sup>55–58</sup> will continue to play a crucial role in converting an ever increasing abundance of possible geometric designs into functional real-world nanomaterials accessible by self-assembly. *Where there is matter, there is geometry* (Johannes Kepler).

## ■ ASSOCIATED CONTENT

### ■ Supporting Information

Self-consistent field theory for block copolymers; spectral method for solving the self-consistent field equations of star-copolymers at intermediate segregation; strong segregation theory; geometric analysis of tricontinuous and columnar mesophases; numerical data of all SCFT phase diagrams. This material is available free of charge via the Internet at <http://pubs.acs.org>.

## ■ AUTHOR INFORMATION

### Corresponding Author

\*E-mail: [Gerd.Schroeder-Turk@fau.de](mailto:Gerd.Schroeder-Turk@fau.de) (G.E.S.-T.).

### Notes

The authors declare no competing financial interest.

## ■ ACKNOWLEDGMENTS

We thank Michael O’Keeffe for insight on crystallographic triple network intergrowths, Mark Matsen for pointing us to the Anderson mixing scheme, and Klaus Mecke for continuing support. G.E.S.-T., J.J.K.K., and M.G.F. acknowledge the hospitality of the Department of Applied Maths at the Australian National University. G.E.S.-T. acknowledges support of the Engineering of Advanced Materials Cluster of Excellence and M.G.F. by the DAAD through the PROMOS program and by the Leonardo college, all at the Friedrich-Alexander University Erlangen-Nürnberg. J.J.K.K. is grateful for the financial support of the Lundbeck Foundation. S.T.H. and L.d.C. acknowledge the Australian Research Council for financial support.

## ■ ADDITIONAL NOTES

<sup>a</sup>The values of  $c/a$  and  $\gamma$  vary with  $\chi N$ ,  $f_X$  and  $\chi_X/\chi$ ; see tables in Supporting Information section V. Note that our SCFT analysis does not include an algorithmic free energy minimization with respect to these parameters but rather extracts these values from a coarse manual sampling.

<sup>b</sup>Strictly speaking, when considering the system as a four-component system of  $A$ ,  $B$ ,  $C$ , and  $X$ , the [8.8.4] tiling corresponds to the [8.8.4.8] tiling.

<sup>c</sup>The interface area  $A_{ABC}$  is the interface area between the species  $A$ ,  $B$ , and  $C$ , as before. Because of the introduction of  $X$ , the value of  $A_{ABC}$  has however changed.

## ■ REFERENCES

- (1) Schoen, A. H. *Interface Focus* **2012**, *2*, 658–668.
- (2) Hyde, S. T.; O’Keeffe, M.; Proserpio, D. M. *Angew. Chem., Int. Ed.* **2008**, *47*, 7996–8000.
- (3) Bockstaller, M. R.; Mickiewicz, R. A.; Thomas, E. L. *Adv. Mater.* **2005**, *17*, 1331–1349.
- (4) Hajduk, D.; Harper, P.; Gruner, S.; Honeker, C.; Kim, G.; Thomas, E.; Fetters, L. *Macromolecules* **1994**, *27*, 4063–4075.
- (5) Schulz, M. F.; Bates, F. S.; Almdal, K.; Mortensen, K. *Phys. Rev. Lett.* **1994**, *73*, 86–89.
- (6) Meuler, A. J.; Hillmyer, M. A.; Bates, F. S. *Macromolecules* **2009**, *42*, 7221–7250.
- (7) Phillips, C. L.; Iacovella, C. R.; Glotzer, S. C. *Soft Matter* **2010**, *6*, 1693–1703.
- (8) Vignolini, S.; Yufa, N. A.; Cunha, P. S.; Guldin, S.; Rushkin, I.; Stefik, M.; Hur, K.; Wiesner, U.; Baumberg, J. J.; Steiner, U. *Adv. Mater.* **2012**, *24*, OP23–OP27.
- (9) Schröder-Turk, G.; Wickham, S.; Averdunk, H.; Large, M.; Poladian, L.; Brink, F.; Fitz Gerald, J.; Hyde, S. T. *J. Struct. Biol.* **2011**, *174*, 290–295.
- (10) Maldovan, M.; Urbas, A. M.; Yufa, N.; Carter, W. C.; Thomas, E. L. *Phys. Rev. B* **2002**, *65*, 165123.
- (11) Saba, M.; Thiel, M.; Turner, M. D.; Hyde, S. T.; Gu, M.; Grosse-Brauckmann, K.; Neshev, D. N.; Mecke, K.; Schröder-Turk, G. E. *Phys. Rev. Lett.* **2011**, *106*, 103902.
- (12) Oh, S. S.; Demetriadou, A.; Wuestner, S.; Hess, O. *Adv. Mater.* **2013**, *25*, 612–617.
- (13) Salvatore, S.; Demetriadou, A.; Vignolini, S.; Oh, S. S.; Wuestner, S.; Yufa, N. A.; Stefik, M.; Wiesner, U.; Baumberg, J. J.; Hess, O.; Steiner, U. *Adv. Mater.* **2013**, *25*, 2713–2716.
- (14) Torquato, S.; Hyun, S.; Donev, A. *Phys. Rev. Lett.* **2002**, *89*, 266601.
- (15) Scherer, M. R. J.; Steiner, U. *Nano Lett.* **2013**, *13*, 3005–3010.
- (16) Crossland, E. J. W.; Kamperman, M.; Nedelcu, M.; Ducati, C.; Wiesner, U.; Smilgies, D. M.; Toombes, G. E. S.; Hillmyer, M. A.; Ludwigs, S.; Steiner, U.; Snaith, H. J. *Nano Lett.* **2009**, *9*, 2807–2812.
- (17) Matsen, M.; Bates, F. *Macromolecules* **1996**, *29*, 7641–7644.
- (18) Hyde, S. T.; de Campo, L.; Oguey, C. *Soft Matter* **2009**, *5*, 2782–2794.
- (19) Elser, V. *Philos. Trans. R. Soc., A* **1996**, *354*, 2071–2075.
- (20) Schoen, A. Infinite Periodic Minimal Surfaces without Self-Intersections; Technical Note TN D-5541, 1970.
- (21) Hyde, S. T.; Oguey, C. *Eur. Phys. J. B* **2000**, *16*, 613–630.
- (22) Hyde, S. T.; Ramsden, S. *Europhys. Lett.* **2000**, *50*, 135–141.
- (23) Hyde, S. T.; Ramsden, S. J.; Di Matteo, T.; Longdell, J. *Solid State Sci.* **2003**, *5*, 35–45.
- (24) Hyde, S. T.; Schröder, G. E. *Curr. Opin. Colloid Interface Sci.* **2003**, *8*, 5–14.
- (25) Evans, M. E.; Robins, V.; Hyde, S. T. *Acta Crystallogr., Sect. A* **2013**, *69*, 241–261.
- (26) Schröder-Turk, G. E.; de Campo, L.; Evans, M. E.; Saba, M.; Kapfer, S. C.; Varslot, T.; Grosse-Brauckmann, K.; Ramsden, S.; Hyde, S. T. *Faraday Discuss.* **2013**, *161*, 215–247.
- (27) Han, Y.; Zhang, D.; Chng, L. L.; Sun, J.; Zhao, L.; Zou, X.; Ying, J. Y. *Nat. Chem.* **2009**, *1*, 123–127.
- (28) Sorenson, G. P.; Schmitt, A. K.; Mahanthappa, M. K. *Soft Matter* **2014**, *10*, 8229–8235.
- (29) Kirkensgaard, J. J. K.; Hyde, S. *Phys. Chem. Chem. Phys.* **2009**, *11*, 2016–2022.
- (30) Gemma, T.; Hatano, A.; Dotera, T. *Macromolecules* **2002**, *35*, 3225–3237.
- (31) Tang, P.; Qiu, F.; Zhang, H.; Yang, Y. *J. Phys. Chem. B* **2004**, *108*, 8434–8438.

- (32) Li, W.; Xu, Y.; Zhang, G.; Qiu, F.; Yang, Y.; Shi, A. *J. Chem. Phys.* **2010**, *133*, 064904.
- (33) Matsushita, Y.; Hayashida, K.; Dotera, T.; Takano, A. *J. Phys.: Condens. Matter* **2011**, *23*, 284111.
- (34) de Campo, L.; Varslot, T.; Moghaddam, M. J.; Kirkensgaard, J. J. K.; Mortensen, K.; Hyde, S. T. *Phys. Chem. Chem. Phys.* **2011**, *13*, 3139–3152.
- (35) Kirkensgaard, J. J. K.; Evans, M. E.; de Campo, L.; Hyde, S. T. *Proc. Natl. Acad. Sci. U. S. A.* **2014**, *111*, 1271–1276.
- (36) O’Keeffe, M.; Peskov, M. A.; Ramsden, S. J.; Yaghi, O. M. *Acc. Chem. Res.* **2008**, *41*, 1782–1789.
- (37) Matsen, M. W.; Schick, M. *Phys. Rev. Lett.* **1994**, *72*, 2660–2663.
- (38) Matsen, M. W. *J. Phys.: Condens. Matter* **2002**, *14*, R21.
- (39) Matsen, M. *Eur. Phys. J. E* **2009**, *30*, 361–369.
- (40) Sioula, S.; Hadjichristidis, N.; Thomas, E. L. *Macromolecules* **1998**, *31*, 5272–5277.
- (41) Bailey, T.; Cordell, M.; Epps, T.; Bates, F. *Macromolecules* **2002**, *35*, 7007–7017.
- (42) Tyler, C. A.; Morse, D. C. *Phys. Rev. Lett.* **2005**, *94*, 208302.
- (43) Hahn, T., Ed. *International Tables For Crystallography*; Kluwer Academic Publishers: Dordrecht, 1992.
- (44) Kirkensgaard, J. J. K.; Pedersen, M. C.; Hyde, S. T. *Soft Matter* **2014**, *10*, 7182–7194.
- (45) Semenov, A. N. *Zh. Eksp. Teor. Fiz.* **1985**, *88*, 1242–1256.
- (46) Helfand, E.; Tagami, Y. *J. Chem. Phys.* **1972**, *56*, 3592–3601.
- (47) Likhtman, A. E.; Semenov, A. N. *Macromolecules* **1994**, *27*, 3103–3106.
- (48) Milner, S. T. *Macromolecules* **1994**, *27*, 2333–2335.
- (49) Likhtman, A. E.; Semenov, A. N. *Macromolecules* **1997**, *30*, 7273–7278.
- (50) Laschat, S.; Baro, A.; Steinke, N.; Giesselmann, F.; Hägele, C.; Scalia, G.; Judele, R.; Kapatsina, E.; Sauer, S.; Schreivogel, A.; Tosoni, M. *Angew. Chem., Int. Ed.* **2007**, *46*, 4832–4887.
- (51) Warren, S. C.; Messina, L. C.; Slaughter, L. S.; Kamperman, M.; Zhou, Q.; Gruner, S. M.; DiSalvo, F. J.; Wiesner, U. *Science* **2008**, *320*, 1748–1752.
- (52) Pisula, W.; Feng, X.; Müllen, K. *Adv. Mater.* **2010**, *22*, 3634–3649.
- (53) Paraschiv, I.; de Lange, K.; Giesbers, M.; van Lagen, B.; Grozema, F. C.; Abellon, R. D.; Siebbeles, L. D. A.; Sudholter, E. J. R.; Zuilhof, H.; Marcelis, A. T. M. *J. Mater. Chem.* **2008**, *18*, 5475–5481.
- (54) Schröder-Turk, G. E.; Fogden, A.; Hyde, S. T. *Eur. Phys. J. B* **2006**, *54*, 509–524.
- (55) Hyde, S. T.; Andersson, S.; Larsson, K.; Blum, Z.; Landh, T.; Lidin, S.; Ninham, B. *The Language of Shape*; Elsevier Science: Amsterdam, 1997.
- (56) Scriven, L. *Nature* **1976**, *263*, 123–125.
- (57) Thomas Edwin, L.; Anderson David, M.; Henkee Chris, S.; Hoffman, D. *Nature* **1988**, *334*, 598–601.
- (58) Andersson, S.; Hyde, S. T.; Larsson, K.; Lidin, S. *Chem. Rev.* **1988**, *88*, 221–242.